Chapter 2

Molecular Gas in the Inner 1 AU of the TW Hya and GM Aur Transitional Disks

This chapter, with minor differences, was published in its entirety under the same title with authors C. Salyk, G. A. Blake, A. C. A. Boogert, and J. M. Brown in *The Astrophysical Journal*, 2007, Volume 655, pp. L105–L108.

2.1 Abstract

We report the detection of CO rovibrational emission from the circumstellar disks around TW Hya and GM Aur. These T Tauri stars have significant mid- to far-IR dust emission but a relative deficit in the near-IR, indicating the presence of an optically thick outer disk but a reduced surface density of small dust grains in the inner disk. Kinematic fits to the resolved emission lines yield inner emission radii of $0.2^{+.4}_{-.05}$ AU for TW Hya and $0.3^{+.2}_{-.15}$ AU for GM Aur, thus the CO v=1→0 emission arises from within the tenuous inner disk. By considering the amount of dust necessary to shield CO from dissociation, we demonstrate that these emission radii are consistent with the inner disk dust populations predicted by SED modeling and K-band interferometry. Rotation diagram analyses yield temperatures that are consistent with our kinematic fits, as well as densities that imply dynamically significant amounts of gas in the inner disk and a gas:small-dust-grain ratio in excess of that in dense clouds. Nevertheless, densities are not high enough to maintain current

accretion rates without replenishment for more than a few hundred years, and transfer of gas from the outer to inner disk is therefore likely required.

2.2 Introduction

As the intersection between star and disk processes and the likely location of terrestrial planet formation, the inner regions of circumstellar disks ($R \lesssim 5$ AU) hold information essential for understanding the evolution of young stars and planetary systems. In particular, inner disk gas controls such varied processes as planetary migration rates (Ward, 1997), orbit circularization (Kominami and Ida, 2002), and accretion (Shu et al., 1994). Because of their small angular scale and proximity to the bright parent star, inner disks are notoriously difficult to image. Recently, however, rovibrational emission lines of species such as H_2O (Carr et al., 2004) and CO have emerged as ideal probes of the near-surface layers of disks. Fundamental CO rovibrational emission (v=1→0) has been observed from embedded protostars (Pontoppidan et al., 2002), classical T Tauri stars (Najita, Carr, & Mathieu 2003; Rettig et al., 2004), and Herbig Ae/Be stars (Brittain et al., 2003; Blake and Boogert, 2004).

CO v=1→0 emission can also provide a unique view into the inner regions of so-called transitional disks, whose spectral energy distributions (SEDs) are characterized by nearly photospheric levels of emission in the near-IR but significant excess flux at mid- to far-IR wavelengths. They are thus believed to have optically thin inner disks or gaps caused by grain growth and/or clearing due to dynamical interactions (Lin and Papaloizou, 1979), perhaps due to the presence of a planet (Rice et al., 2003; Calvet et al., 2002). Two prototypical examples of transitional disks are TW Hya [K8V] and GM Aur [K5V], whose SEDs show evidence for significant disk clearing out to ~ 4 AU (Calvet et al., 2002) and ~ 24 AU (Rice et al., 2003), respectively. For TW Hya, SED modeling yields an inner disk dust mass estimate of $\sim 6\times10^{-3}$ $M_\oplus$ (Calvet et al., 2002), while a K-band interferometric study yields values closer to $\sim 5\times10^{-7}$ $M_\oplus$ (Eisner, Chiang, & Hillenbrand 2006). There is an estimated 2.5×10^{-4} $M_\oplus$ of dust encircling GM Aur, confined to within ~ 5 AU from the star (Calvet et al., 2005). Accretion rates for TW Hya and GM Aur are lower than that of average

T Tauri stars: $\sim 4{\times}10^{-10}$ $M_{\odot}\mathrm{yr}^{-1}$ (Muzerolle et al., 2000) and $\sim 10^{-8}$ $M_{\odot}\mathrm{yr}^{-1}$ (White and Ghez, 2001).

Observations of CO v=1→0 emission from TW Hya were first reported by Rettig et al. (2004). We expand on these results, reporting NIRSPEC observations of CO emission from TW Hya that cover a larger range of rotational energies, ($E_{\mathrm{up}} \sim$ 3000–6000 K versus $\sim$ 3200–4700 K), as well as Phoenix observations for which the emission lines are spectrally resolved. We also report the first observations of CO v=1→0 emission from GM Aur.

2.3 Observations

M-band spectra were obtained with NIRSPEC (McLean et al., 1998) at the Keck II telescope on 2005 April 24–25 and 2005 December 18, 20 for TW Hya, and 2004 December 27, 30 for GM Aur. Echelle mode observations with the $0.43'' \times 24''$ slit (yielding a Gaussian FWHM of $\sim$ 12.5 km s^{-1}, as measured on unresolved CO absorption lines) encompassed the first two R-branch and many P-branch lines [specifically P(1→12) and P(30→40)] of the v=1→0 CO rovibrational band. Further Phoenix (Hinkle et al., 2003) spectra of a few TW Hya lines were obtained at Gemini South on 2006 April 06–07 using the $0.25'' \times 14''$ slit (measured FWHM $\sim$ 5 km s^{-1}).

The 2D echellograms were analyzed with the procedures outlined in Boogert et al. (2002), using nearby standard stars (HR1620 [A7V], HR4313 [A2V], HR4494 [B9V], and, for Gemini data, HR5028 [A2V]) for atmospheric correction and flux calibration. After removal of wavelengths with significant telluric absorption (transmission $\lesssim$ 40–65%), flux calibrated spectra with signal-to-noise ratios approaching the shot noise limit can be obtained. For TW Hya, which was observed twice with Doppler shifts of $\sim$ 12 and $\sim$ 24 km s^{-1}, most line profiles remain complete after the removal of potential telluric interference. For GM Aur, observed only once with a Doppler shift of $\sim$ 11 km s^{-1}, line profiles are incomplete. However, more than half of the profile remains, allowing reasonable constraints on both the height and width of the lines. Although previous results reported line-to-continuum variability by a factor of 10 or more for TW Hya (Rettig et al., 2004), we saw variations consistent with noise, with line-to-continuum ratios varying from 0.6–1 (for the P(5)–P(7) lines).

TW Hya shows CO v=1→0 R(0–1), P(1–12) and P(30–32) lines. GM Aur was observed in one additional setting and its spectrum shows emission out to at least P(14). No ^{13}CO v=1→0 or CO v=2→1 emission is seen. The line and continuum spatial FWHM of $\sim 0.5''$ are consistent with the 0.4–0.7″ K-band seeing, and constrain the emission to radii < 10–15 AU for TW Hya and < 30–35 AU for GM Aur. Excerpts of our NIRSPEC M-band spectra are shown in Figure 2.1.

2.4 Results

2.4.1 Line Widths

Because CO v=1→0 emission originates from the inner regions of Keplerian disks, the line shapes depend on the disk inclination and emitting radii (Najita et al., 2003; Blake and Boogert, 2004). For TW Hya's nearly face-on disk, the NIRSPEC data yield only marginally resolved lines, so we instead utilize the R=60,000 Phoenix spectra. A composite lineshape from the P(6)–P(9) transitions is presented as an insert in Figure 2.1. Individual lines were velocity centered, continuum subtracted, normalized, and resampled into 2 km s^{-1} bins.

Inner emission radii are often estimated by measuring the velocity of the Half Width at Zero Intensity (HWZI). This procedure yields an inner radius for TW Hya of $\sim$ 0.04 AU (for $M_\star$=0.6 $M_\odot$ and i=7° ± 1°, Qi et al. 2004), but does not take into account the effect of disk structure or of any non-Keplerian (turbulent) motions, whose line-of-sight projections are especially important for low-inclination disks. A complete 2-D disk model would be difficult to constrain with only the data shown here, and we therefore present a compromise—a disk model consisting of an optically thick dust layer and overlying hotter gas layer, each with T=$T_0\,(r/\mathrm{AU})^\alpha\,(L/L_\odot)$. Based on SED fits using the radiative transfer models of Dullemond et al. (2002), and on matching total line fluxes, we chose the following model parameters: T_0(dust)=345 K, T_0(gas)=440K, α=−0.2, and r_{out}=2 AU. Stellar and disk parameters—M and i as above, L=0.25 $L_\odot$ (Thi, van Zadelhoff & van Dishoeck, 2004) — are derived from other studies, and v_{Turb} is parameterized as $0.01 v_{\mathrm{Kep}}$. The resultant line shapes were then convolved with the known Phoenix instrument response function (IRF).

The best least-squares fit was achieved with $r_{\rm in}$=0.2 AU. Including all trials within the χ^2 95% confidence interval, with σ defined by the flux variation beyond the line profile wings, inner radii consistent with the data are $r_{\rm in}=0.2^{+0.2}_{-0.05}$. Note that this estimate is several times larger than that estimated from the HWZI. An investigation of all of the disk parameters that could influence estimates of $r_{\rm in}$ is not possible with this dataset; nevertheless, we tried to get a feel for the magnitude of the importance of a few key parameters.

For nearly face-on disks such as TW Hya, the turbulent velocity is the most influential parameter at fixed inclination. For example, with $v_{\rm Turb} \sim 0.05 v_{\rm Kep}$ the best-fit radii are $\sim$ 1 AU, but at such distances the disk may be too cool to induce the observed line fluxes. Doppler broadening at the temperatures of interest is unimportant, but the temperature gradient can be significant. Tests with α=$-$0.44 and $-$0.05 result in $r_{\rm in}$ up to 0.4 AU. To reflect this uncertainty, true error bars should be larger than the χ^2 estimate by a factor of a few. Because the inclination of TW Hya's outer disk is well-constrained this turns out to be a relatively insignificant source of error, affecting $r_{\rm in}$ by $\lesssim$ 40%, unless the disk is strongly warped.

The CO emission lines from GM Aur have a FWHM of $\sim$ 30 km s^{-1}, and so the NIRSPEC IRF makes a minor contribution to the measured line profile. A composite line was created utilizing P(9)–P(12) and P(14) (see Figure 2.1 insert), and a HWZI estimate yields an inner emission radius of 0.1 AU (with M=0.84 $M_\odot$, i=54° ± 5°; Simon et al. 2001). Utilizing our two-layer disk model with the same parameterization as for TW Hya, with stellar mass and disk inclination as above, and with L=0.74 $L_\odot$, $r_{\rm out}$=5 AU, we find that $r_{\rm in}$=0.3 AU. A χ^2 95% confidence interval metric yields $r_{\rm in}=0.3^{+0.2}_{-0.15}$. The turbulent velocity in this case is much less significant, but changes in α can still affect $r_{\rm in}$ by factors of $\sim$ 2. Inclination errors have little effect ($\lesssim$ 15%) on $r_{\rm in}$.

2.4.2 Excitation Diagrams

To estimate the gas temperatures and mass surface densities, we construct excitation diagrams, in which $\ln\left(F_{ji}/(g_j A_{ji} \nu_{ji})\right)$ is plotted against E_j. Here, F_{ji} is the line flux, A_{ji} is the spontaneous emission coefficient, ν_{ji} is the wavenumber of the transition, $g_j (= 2j+1)$ is the degeneracy of the

upper state and E_j is the upper state energy. For optically thin, single-temperature emission the dependence is linear, with a slope of $-1/T$, where T is the excitation temperature that characterizes the rotational manifold, and an intercept that yields the column density. Nonlinear dependencies can indicate temperature gradients or optically thick emission.

Before calculating line fluxes, we first estimate the reduction in observed line fluxes induced by absorption features in the photospheres of TW Hya and GM Aur. Although these photospheres are nearly unobstructed at 1 μm (Edwards et al., 2006), in the M-band veiling appears to dominate. We quantify this effect by assuming that away from the v=1→0 CO lines the spectrum is the sum of a constant veiling term plus a scaled photospheric template, given by NIRSPEC data for the [K7V] star HD 79211 (see Figure 2.1). The veiling and median photospheric contributions are 0.197±0.006, 0.096±0.006 Jy for TW Hya and 0.081±0.002, 0.019±0.002 Jy for GM Aur. Here the error bars reflect only the statistical uncertainties of the fit. Subtraction of the photosphere+veiling model should now yield the "true" disk line fluxes. For TW Hya, R(1)–R(0) and P(1)–P(12) transition fluxes are changed by $\sim 6\%$ on average, but P(30)–P(32) fluxes by $\sim 30\%$. For GM Aur, the moderate S/N and the dominance of veiling render flux corrections insignificant. (The model fluctuations are of order 0.001 Jy, while the noise level for GM Aur is $\sim$ 0.01 Jy).

If HD 79211 is not a proper template, or if TW Hya's or GM Aur's photospheric absorption lines are filled in by hot gas from the inner disk or accretion flow, our fits will tend to underestimate the photospheric contribution. Therefore, to provide an upper limit to the possible photospheric impact, we considered the case where the spectra between the CO v=1 → 0 emission lines are assumed to be "veiling free". Specifically, the model photosphere was scaled such that its median matched that of the source spectrum and was then subtracted from the data to derive veiling-free fluxes. Again, the GM Aur line fluxes are not significantly affected because the variations in the reference photosphere ($\sigma \sim 0.007$ Jy) are smaller than the noise level of the spectrum. TW Hya R and P(1)–P(12) line fluxes are changed by 7%, on average, while P(30)–P(32) fluxes are increased by up to 160%.

The rotation diagram in Figure 2.2 includes fluxes of 17 identifiable emission lines for TW Hya and 12 for GM Aur. Line fluxes are shown in Table 2.1. Raw fluxes are displayed as squares and

fluxes corrected by a veiling+photosphere model are displayed as diamonds. Additionally, we show upper limits for GM Aur and veiling-free fluxes for TW Hya. (For clarity, we show only one set of fluxes at low energies). Error bars include two contributions added in quadrature: one derived from the standard deviation of the continuum flux and the other derived from the standard deviation of fit line widths.

The most obvious feature of these plots is that they are nonlinear; therefore, the optically thin, isothermal assumption is invalid. To fully model the line emission, one would need to consider both the gas and dust distributions and temperatures as well as the disk geometry. However, to derive a simpler, more intuitive estimate of conditions, we fit our rotation diagrams with a constant dust continuum plus a single temperature gas whose column density, rotational temperature, and emitting area are free parameters. Gaussian line shapes derived from the data are also provided to the model.

The best fit to TW Hya's veiling+photosphere corrected fluxes can be seen in Figure 2.2. Error bars are defined by the range of models within a 95% χ^2 confidence interval, plus an upper density limit provided by the non-detection of ^{13}CO (see top of Figure 2.2). Note that Area and N tend to covary, and are both anti-correlated with T, such that fits with high T correspond to low N and Area, and vice-versa. The veiling-free fluxes (representing an upper limit) give only a slightly different temperature and area: $\log(N)=-3.7^{+0.5}_{-0.4}\,\mathrm{g\,cm^{-2}}$, $\mathrm{T}=950^{+550}_{-300}\,\mathrm{K}$, and $\log(\mathrm{Area})=-2.3^{+0.6}_{-0.6}\,\mathrm{AU}^2$. A lower temperature and density (T=430±40 K, $N\sim1\times10^{-8}\,\mathrm{g\,cm^{-2}}$) were derived by Rettig et al. (2004), assuming optically thin lines and an emitting area equal to that sampled by NIRSPEC (i.e., out to several tens of AU). However, given the curvature below $\sim$ 3300 K in Figure 2.2 and the high temperatures required to excite the transitions, these assumptions are not appropriate. For graybodies, our fit temperatures correspond to $r=0.07^{+0.36}_{-0.05}\,\mathrm{AU}$ and $0.04^{+0.39}_{-0.03}\,\mathrm{AU}$, but warm gas can exist at larger radii in disks with super-heated atmospheres (e.g., Kamp and Dullemond, 2004).

Best fits for GM Aur can also be seen in Figure 2.2. In this case, the χ^2 interval is significantly larger and we used three additional limits to constrain our fits — an upper flux limit based on non-detection of emission at high energies, a density limit imposed by non-detection of ^{13}CO and

a requirement that fit models have significant curvature at low energies. The best-fit temperature corresponds to r=$0.53^{+0.94}_{-0.16}$ AU for graybodies.

2.5 Discussion

The molecular emission we observe originates from inside 1 AU—well inside the estimated disk transition radii of ~ 4 and ~ 24 AU for TW Hya and GM Aur. Line profiles yield inner radii of $0.2^{+0.4}_{-0.05}$ and $0.3^{+0.2}_{-0.15}$ AU, and rotational temperatures are consistent with emission radii of r=$0.07^{+0.36}_{-0.05}$ and r=$0.53^{+0.94}_{-0.16}$ AU for equilibrium graybodies. The consistency between the emission radii and inner radii suggests that the CO emitting layer has temperatures similar to those for graybodies in equilibrium with the stellar radiation field.

Although the CO lies inside the optically thick transition radius derived from SEDs, it lies outside the estimated disk truncation and dust destruction radii. For example, Keck interferometry plus IR photometry yield an inner radius of 0.06 ± 0.01 AU for TW Hya's dust disk, which is consistent with an estimate of the magnetic truncation radius (Eisner et al., 2006). GM Aur's inner disk dust is truncated at $0.221^{+0.082}_{-0.085}$ AU, consistent with the dust sublimation radius (Akeson et al., 2005a). In both cases, our measurements put the CO inner radius outside that of the dust. This is expected because the CO must be shielded from photodissociation; at our derived inner radii, radial vacuum-UV ($\lambda$$\sim$0.1 μm) optical depths are $>$ 5–10 according to dust ($\kappa = 10^3\,(\nu/\nu_k)\,\mathrm{cm^2 g^{-1}}$) and disk mass surface density ($\Sigma = \Sigma_0\,(R/\mathrm{AU})^{-3/2}$) models analogous to those in Eisner et al. (2006).

Column densities derived from fits to the rotational diagrams allow us to estimate the gas content in the inner disk and the gas-to-dust ratio. The best fit to TW Hya's rotation diagram yields a gas surface density of $\Sigma_{gas}$$\sim$$0.07\,\mathrm{g\,cm^{-2}}$ for an H_2/CO ratio of 5×10^3 (Lacy et al., 1994). (This molecular ratio, observed toward massive protostars, is among the lowest observed in the dense ISM, and thus should provide a reasonable lower limit to the total gas mass.) A comparison with dust column densities derived by Eisner et al. (2006) for TW Hya implies a gas-to-dust ratio of $\sim 10^4$ at $\sim$ 0.2 AU; a comparison with the much higher dust surface density derived from Calvet et al. (2002) implies a gas-to-dust ratio of $\sim$ 20. If we extrapolate our densities to 4 AU with a surface density

that scales as $r^{-1.5}$ we predict a total inner disk gas mass of 3×10^{25} g ($0.005\,M_{\oplus}$).

The best fit to GM Aur's CO emission yields a gas surface density of $\Sigma_{gas} \sim 0.1$ g cm^{-2}. Extrapolating to 5 AU yields a total inner disk gas mass of 3×10^{25} g ($0.005\,M_{\oplus}$). Given the total dust mass from Calvet et al. (2005), this implies a gas-to-dust ratio of ~ 70.

The inner disk mass could only sustain the observed accretion rate for tens of years or less without invoking transfer of material from the outer disk. Steady mass transfer across gaps may be caused by an embedded planet (Rice et al., 2003). Interestingly, the derived gas surface densities also approximate those shown to provide significant circularization of the orbits of planetary embryos in the terrestrial planet-forming region (of order 0.1–1 g cm^{-2} at 1 AU; Kominami and Ida, 2002), and so may play an important role in shaping the dynamics of any forming planetesimals.

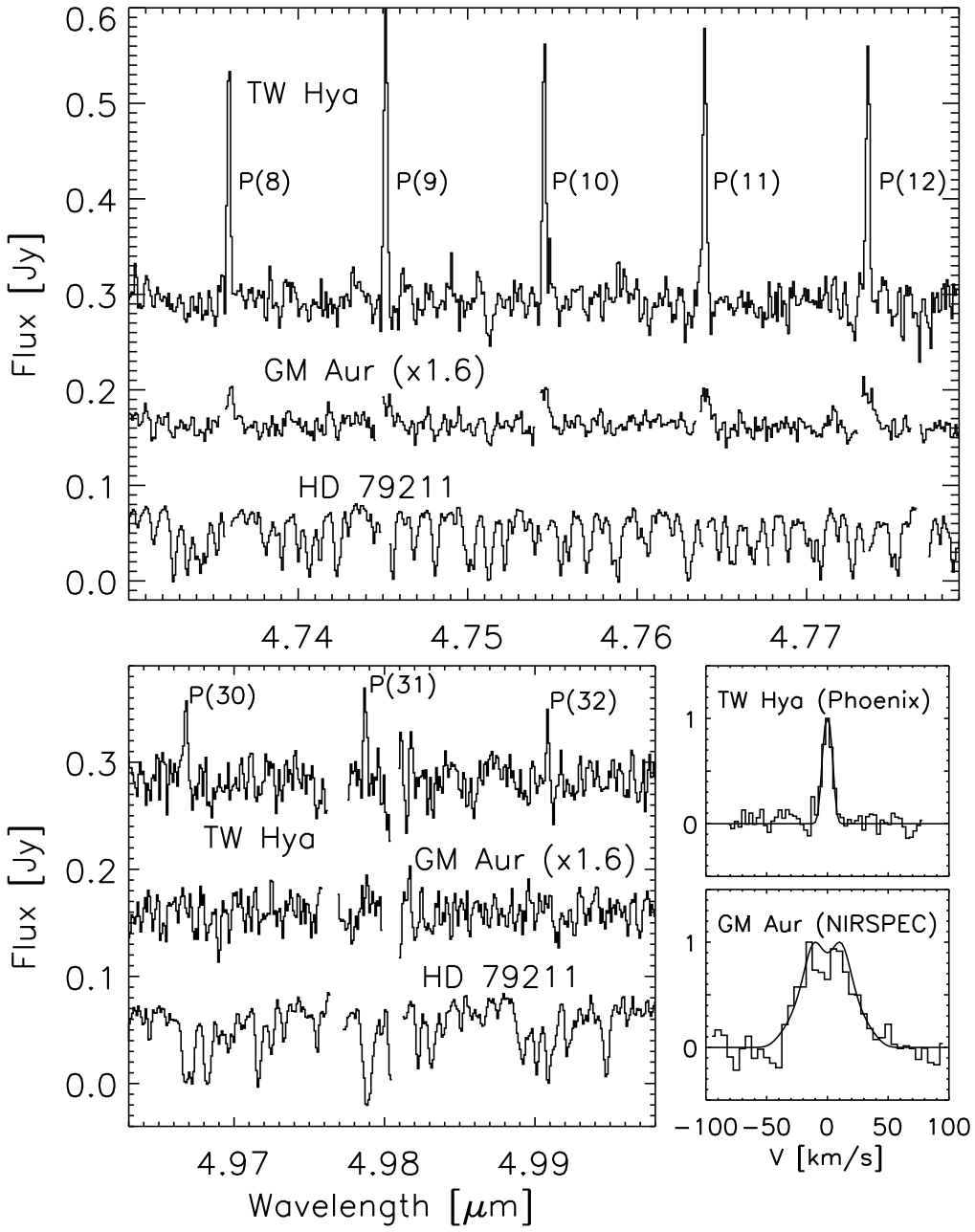

Figure 2.1: Excerpts of the NIRSPEC spectra of TW Hya and GM Aur. The HD 79211 spectrum has been normalized to TW Hya's continuum and offset. Line composites are shown at lower right, with the best two-layer disk model overlain.

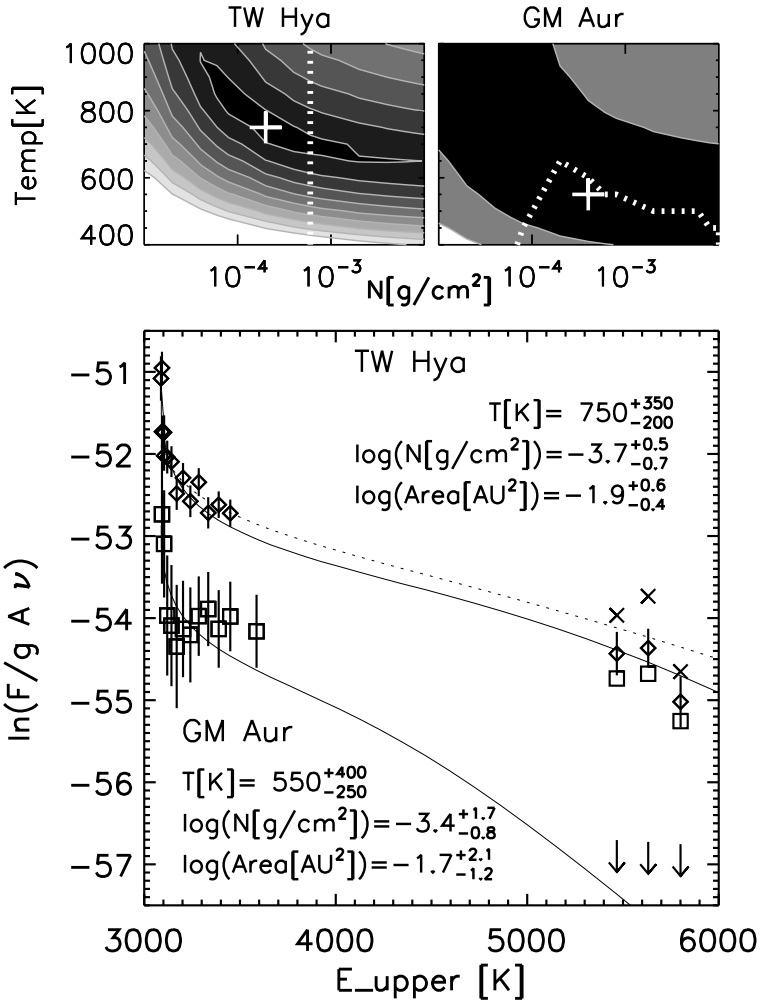

Figure 2.2: Rotation diagrams for TW Hya and GM Aur. Raw data are shown as squares, photospheric plus veiling-corrected fluxes as diamonds, and veiling-free fluxes as crosses. Arrows denote upper limits and best model fits are shown as solid lines (dashed line for veiling-free fluxes). Above we show the fit χ^2 contours for column density and temperature with area fixed at best-fit value. The innermost contour depicts the 95% confidence interval; subsequent contours are integer multiples of this critical χ^2 value. Additional constraints are shown as dotted lines. The quoted limits are the *ranges* of the correlated fit parameters consistent with the data.

Table 2.1. Line Fluxes

transition	TW Hya F_0	FWHM	F_c	FWHM	F_{nv}	FWHM	GM Aur F_0	FWHM
R(1)	5.0 ± 1.0	14.5	5.1 ± 1.3	14.6	5.4 ± 1.3	15.0	1.3 ± 0.9	22.8
R(0)	5.5 ± 1.1	15.5	5.5 ± 1.3	15.1	5.6 ± 1.4	14.6	0.9 ± 0.8	15.6
P(1)	2.9 ± 0.8	16.8	4.8 ± 1.1	22.8	3.7 ± 1.0	15.0	···	···
P(2)	5.2 ± 1.0	20.7	5.0 ± 1.1	20.8	5.0 ± 1.1	22.2	···	···
P(3)	5.9 ± 1.1	21.0	5.5 ± 1.2	20.3	5.1 ± 1.1	19.5	···	···
P(4)	7.1 ± 1.4	13.5	7.2 ± 1.8	13.6	7.5 ± 1.8	13.9	1.0 ± 0.8	19.6
P(5)	8.3 ± 1.6	14.2	8.4 ± 2.0	14.3	8.5 ± 2.0	14.5	1.1 ± 0.8	18.0
P(6)	6.7 ± 1.3	13.8	6.8 ± 1.7	13.9	7.0 ± 1.7	14.0	1.1 ± 0.8	18.0
P(7)	9.5 ± 1.7	14.5	9.5 ± 2.2	14.7	9.8 ± 2.2	15.2	1.5 ± 0.9	26.9
P(8)	8.3 ± 1.6	13.6	8.1 ± 2.0	13.4	7.9 ± 2.0	13.1	1.6 ± 0.9	25.4
P(9)	11.3 ± 1.9	15.3	11.5 ± 2.5	15.5	11.9 ± 2.5	15.9	2.2 ± 1.1	37.2
P(10)	8.8 ± 1.7	13.8	8.7 ± 2.1	13.7	8.5 ± 2.1	13.4	2.7 ± 1.2	44.6
P(11)	10.6 ± 1.7	16.5	10.5 ± 2.2	16.2	10.3 ± 2.2	15.8	2.3 ± 1.1	35.6
P(12)	9.9 ± 1.7	16.0	10.2 ± 2.1	16.2	10.7 ± 2.2	16.6	2.9 ± 1.2	42.9
P(14)	···	···	···	···	···	···	2.8 ± 1.2	46.3
P(30)	2.9 ± 0.8	18.5	3.9 ± 1.0	21.4	6.3 ± 1.2	26.5	···	···
P(31)	3.1 ± 0.7	15.6	4.3 ± 1.0	18.2	8.1 ± 1.3	27.1	···	···
P(32)	1.8 ± 0.6	11.8	2.3 ± 0.7	12.6	3.3 ± 0.9	14.0	···	···

Notes: All fluxes are in 10^{-18} W m^{-2}. Error bars include two contributions added in quadrature: one derived from the standard deviation of the continuum flux and the other derived from the standard deviation of fit line widths. F_0 is the flux with no photospheric corrections. F_c is photospheric+veiling adjusted flux. F_{nv} is the flux adjusted with a model assuming no veiling contribution. Line FWHMs for each set of fluxes are also given in km s^{-1}.